Structural basis for oligomerization and glycosaminoglycan-binding of CCL5 and CCL3

Wenguang G Liang[1], Catherine G. Triandafillou[2], Teng-Yi Huang[3], Medel Manuel L. Zulueta[3], Shiladitya Banerjee[4], Aaron R. Dinner[4,5], Shang-Cheng Hung[3*], Wei-Jen Tang[1*]

[1]Ben-May Department for Cancer Research, The University of Chicago

[2]Biophysics program, The University of Chicago

[3]Genomics Research Center, Academia Sinica, Taipei, Taiwan

[4]James Franck Institute, The University of Chicago

[5]Department of Chemistry, The University of Chicago

[*]Corresponding Authors: WJT: wtang@uchicago.edu; SCH: schung@gate.sinica.edu.tw.

Short title: GAG-free and GAG-bound CCL3 and CCL5 oligomers

Key words: Signal transduction, CC chemokine, protein oligomerization, glycosaminoglycan, X-ray crystallography

Accession numbers: The coordinates and structure factors have been deposited in Protein Data Bank (http://www.pdb.org) with accession code 5CMD (CCL5 oligomer), 5COY (CCL5 dimer), 5DNF (CCL5 oligomer-GAG-8f complex), 5D65 (CCL3 oligomer-GAG-8f complex), and 5COR (CCL3 oligomer with N-termini pointing outward).

Supplemental information: Supplemental information includes supplemental methods, 6 figures, 2 tables, and a 3D Molecular movie.

Author contributions: W.G.L, W.J.T. designed and performed research and analyzed the data. C.G.T., S.B., and A.R.D. developed the mathematical model and analyzed SAXS data. D.Y.H., M.M.L.Z., and S.C.H. contributed synthetic heparin. W.G.L. C.G.T., and W.J.T. wrote the paper and all authors edited the paper.

Abstract

CC chemokine Ligand 5 (CCL5) and CCL3 are critical for immune surveillance and inflammation. Consequently, they are linked to the pathogenesis of many inflammatory conditions and are therapeutic targets. Oligomerization and glycosaminoglycan (GAG)-binding of CCL5 and CCL3 are vital for the functions of these chemokines. Our structural and biophysical analyses of human CCL5 reveal that CCL5 oligomerization is a polymerization process in which CCL5 forms rod-shaped, double helical oligomers. This CCL5 structure explains mutational data and offers a unified mechanism for CCL3, CCL4, and CCL5 assembly into high molecular weight, polydisperse oligomers. A conserved, positively charged BBXB motif is key for the binding of CC chemokines to GAG. However, this motif is partially buried when CCL3, CCL4, and CCL5 are oligomerized; thus, the mechanism by which GAG binds these chemokine oligomers has been elusive. Our structures of GAG-bound CCL5 and CCL3 oligomers reveal that these chemokine oligomers have distinct GAG-binding mechanisms. The CCL5 oligomer utilizes another positively charged and fully exposed motif, KKWVR, in GAG-binding. However, residues from two partially buried BBXB motifs along with other residues combine to form a GAG-binding groove in the CCL3 oligomer. The N-termini of CC chemokines are shown to be involved in receptor binding and oligomerization. We also report an alternative CCL3 oligomer structure which reveals how conformational changes in CCL3 N-termini profoundly alter its surface properties and dimer-dimer interactions to affect GAG binding and oligomerization. Such complexity in oligomerization and GAG binding enables intricate, physiologically relevant regulation of CC chemokine functions.

Significance

Oligomerization and GAG binding are key regulatory steps for many extracellular ligands. Our analyses provide a structural basis of CCL5 and CCL3 oligomerization and explain how oligomerization affects the interaction of these chemokines with GAG and their functions. Our GAG-bound chemokine structures reveal how CCL5 and CCL3 oligomerization creates distinctive GAG-binding grooves to enhance GAG binding via avidity for regulating chemokine functions. Furthermore, our CCL5 structure may explain how CXCL4, a CXC chemokine, heterooligomerizes with CCL5 to modulate chemokine-mediated activities. Together, these data provide new structural insights into how oligomerization and GAG binding are coupled to regulate functions of CC chemokines and offer novel pharmacophores for the design of therapeutics for treating chemokine-mediated human diseases.

\body

Introduction

CC chemokines are a 28-member family of 8-14 kDa small molecular weight (MW) chemotactic cytokines with crucial roles in inflammation and infection (1, 2). Chemokine oligomerization and their interaction with glycosaminoglycans (GAGs), polysaccharides that are either free or attached to proteoglycans mostly on cell surface or in the extracellular matrix, is a coupled process that play key roles in chemokine functions (3-8). These include, but are not limited to, protection from proteolysis, regulation of chemotactic/haptatactic gradients to guide cell migration, transcytosis of chemokines across cells, and presentation to surface receptors of target cells, particularly under flow conditions. Most CC chemokines readily dimerize by themselves, and form higher MW complexes in the presence of GAGs (4). CCL3 (MIP-1α), CCL4 (MIP-1β), and CCL5 (RANTES) are CCR5 ligands that are involved in diverse proinflammatory responses and are targeted for therapeutic innovations for human diseases including cancer, cardiovascular diseases, and HIV infection (9-12). Unlike other CC chemokines, these chemokines reversibly self-assemble into high MW oligomers, up to >600 kDa in size (13, 14). The presence of GAGs further modulates the oligomerization of these chemokines. Mutants of these chemokines with reduced oligomerization have chemotactic activity comparable to wild type chemokines (15, 16). However, such mutants make CCL3, CCL4, and CCL5 less effective at recruiting cells into the mouse peritoneum (14, 17, 18). CCL5 mutants defective in oligomerization fail to block HIV infection and induce the expression of interferon-γ and CCL4 (15, 19). Normally, CCL5 can trigger CCR5-dependent apoptosis and GPCR-independent MAP kinase activation via CD44, but CCL5 mutants defective in either oligomerization or GAG binding fail to elicit these responses (20, 21). Manipulation of CCL3 oligomerization by mutation has led to the development of CCL3-based cancer therapies that preserve stem cells and boost immune therapy (11, 12, 22).

Accumulating evidence indicates that oligomerization of CC chemokines occurs *in vivo*. For example, CCL5 is released from T cells as high MW, GAG-bound complexes (23) and filamentous CCL5 oligomers are found on vascular endothelial cells in a GAG-dependent manner (24). However, significant gaps exist in our understanding of the structural basis of CC chemokine oligomerization and GAG binding. While CCL3, CCL4, and CCL5 oligomerize readily under physiological conditions, only CCL3 and CCL4 oligomer structures are available

at a neutral pH (14) (Table S1). All available CCL5 structures were determined at acidic pH (25-30) (Table S1). Unfortunately, none explain how CCL5 mutations profoundly affect CCL5 oligomerization and alter its biological functions (15, 16, 18-21, 31). Thus, the structural basis for CCL5 oligomerization is unknown.

Significant efforts have been made to elucidate the structural basis of GAG binding to target proteins (3, 32, 33). Such efforts reveal the structural diversity of GAGs, their target proteins, and the interaction interfaces between them. Mutational and structural studies have confirmed a role of the BBXB motif (basic/basic/x/basic residue) in CC chemokines in GAG binding, oligomerization, and receptor binding (4, 5, 14, 28, 34). Structures of CCL3 and CCL4 oligomers, however, show that the BBXB motif is located at the interface between dimers of these chemokines (14). Thus, oligomerization prevents the BBXB motif from binding GAG in the manner shown in the CCL5-GAG disaccharide structure (28). Thus, how GAG binds CC chemokine oligomers and how chemokine oligomerization affects GAG binding remains unknown. Here, we combined crystallographic, SAXS, and mathematical modeling analyses to unveil the structural basis for CCL5 oligomerization at a physiological pH. We also solved the structures of CCL3 and CCL5 oligomers in complex with synthetic heparin to elucidate the molecular basis for the interaction of CC chemokine oligomers with GAG.

Results

Structural basis of CCL5 oligomerization: To address the structural basis for CCL5 oligomerization, we sought to identify a crystallization condition for CCL5 at neutral pH (Table S2). We found that the naturally occurring CCL5(4-68) variant of CCL5, in which three CCL5 N-terminal residues are deleted, displays dramatically reduced CCL5 precipitation without affecting formation of high MW oligomers. While CCL5(4-68) could be crystalized at an acidic pH, it also formed crystals at a pH of 7.0-8.0 that was temperature sensitive (optimal at 30^{o}C). Heparins, a well-known class of GAGs, have disaccharide repeats of glucosamine-iduronic acid or glucosamine-glucuronic acid that have 48 possible combinations (33). 23 of 48 possible repeats have been found *in vivo*. To determine a GAG-bound CCL5 oligomer structure, we used synthetic heparins that have one to four N,O6-disulfoglucosamine (SGN) and O2-sulfoiduronic acid (IDS) repeats (Figure S1A) (33, 35, 36). The use of synthetic heparin eliminated the complexity and chemical heterogeneity of commercially available GAGs and allowed the formation of better diffracting crystals that had interpretable GAG density. We first

solved the dimeric CCL5(4-68) structure crystallized at an acidic pH at 1.4Å resolution, then used it as a search model for molecular replacement. In conjunction with sulfur phasing, we solved the structure of CCL5(4-68) oligomer crystallized at a neutral pH in the presence and absence of heparin **8f**, a synthetic heparin octasaccharide (Figure S1A) at 2.55Å and 3.05Å resolution, respectively (Table S2). The week-long dehydration of CCL5(4-68) crystals in the presence of **8f** significantly improved diffraction quality.

The electron density of CCL5 is generally excellent except for the 4-10 N-terminal loop (Figure S1B). The structure of heparin-free CCL5(4-68) is a hexamer in an asymmetric unit (Figure 1A), while that of heparin **8f**-bound CCL5(4-68) has nine monomers arranged as one and a half hexamers (Figure S1C). These hexameric structures are nearly identical (Figure S1D). The CCL5 hexamer can be viewed as a complex of three CCL5 dimers. Within the hexamer, the CCL5 monomer has an expected structure: a N-terminal segment (aa 4-20) followed by a 3_{10} helical turn (aa 21-23), an anti-parallel three-stranded β-sheet (aa 24-55), and an α-helix (aa 55-68). The arrangement of CCL5 dimers is similar to dimeric CCL5 structures crystallized at low pH (Figure S1E-F) (25-30). However, the contacts between CCL5 dimers in our CCL5 oligomeric structure nicely explain how mutations affect CCL5 oligomerization and function. Between CCL5 dimers, E26 forms a salt bridge with R47 while E66 forms hydrogen bonds with T43 and R44 as well as a salt bridge with K45 (Figure 1B). This explains how the mutation of E66 or E26 to serine or alanine profoundly reduces CCL5 oligomerization and decreases its functionality while mutations at the ^{44}RKNR^{47} BBXB motif also affect CCL5 oligomerization (Figure S1G) (15, 16, 18-21). This structure also explains how the A22K mutation enhances CCL5 oligomerization, since this lysine would form a hydrogen bond to N63 of the adjacent CCL5 monomer (Figure S1H) (31). This structure can explain how an H23K mutation reduces CCL5 oligomerization by disrupting van der Waals contacts between H23 and N63 of the two CCL5 monomers (31).

The mechanism for forming double helical CCL5 oligomers is similar to that of CCL3 and CCL4 oligomers: The structure of CCL5(4-68) hexamer suggests that, like CCL3 and CCL4, charge and surface complementarity allow CCL5 dimers to come together and polymerize into rod-shaped double helical oligomers that are polydisperse in size (Figure 1C-D) (14). Residues that form hydrophilic interactions at the dimer-dimer interfaces are highly conserved between CCL3, CCL4 and CCL5, but not other CC chemokines (Figure 1E, S1I-J). This can explain why only these chemokines self-assemble into high MW oligomers. To probe

whether wild type CCL5 forms rod-shaped oligomers in solution, we performed SAXS analysis of CCL5 (0.5-1 mg/mL) in buffer containing Tris-HCl (pH=8) and 500 mM NaCl to prevent CCL5 from precipitating (Figure 2A). If CCL5 oligomers were rod-shaped, the linearity over a range of scattering vectors in the plot of cross-section, Guinier rod would be expected. Indeed, the observed plot revealed linearity at q values ranging from 0.03 to 0.09 (Figure 2A inset).

There are three available CCL5 oligomeric structures: a double helical rod based on our CCL5(4-68) structure (PDB=5CMD), a CCL5 structure derived from a hybrid method using NMR, SAXS and molecular simulation (PDB=2L9H), and P2-RANTES, which has enhanced the ability of CCL5 to inhibit HIV-1 infection due to its mutated N-terminal sequences (PDE=2VXW) (27, 29). All of them are rod-shaped. We first generated a oligomer model from each of the three structures that best fit the experimental R_g values and had χ values near 1 (Figure 2A). We then evaluated which model best fit the experimental cross-section R_g value (R_c). We found that only the double helical CCL5 26mer derived from our CCL5(4-68) model fit the experimental scattering curves and R_c value well (Figure 2A). While the CCL5 26mer offered the best fit among the three models, the predicted maximal dimension (D_{max}) of the CCL5 26mer (250 Å) deviated significantly from the observed D_{max} value of CCL5 (350 Å, Figure 2A). We rationalize that CCL5 follows a simple polymerization mechanism, and thus should exist as an equilibrium mixture of monomers, dimers, and oligomers of different lengths (14, 37). Indeed, this model generated a pair distribution profile that fit well with the observed P(r) distribution (Figure 2A). Together with existing mutational studies (15, 16, 18-21), we conclude that our double helical CCL5 oligomer model represents how CCL5 forms polydisperse oligomers in solution under physiological conditions (Figure S1G). This could also represent CCL5 filaments found on the surface of endothelial cells that are polydisperse in size (24).

Under the same experimental conditions, we found that CCL3 had a much smaller R_g (38Å) than wild type CCL5 (88Å) (Figure 2B). We speculate that the additional hydrophobic contacts in CCL5 could render CCL5 more prone to form high MW oligomers than CCL3 (Figure 1E). The R_g value of CCL3 was also much smaller than that of CCL3 observed in phosphate buffered saline (pH 7.2), which had an R_g value of 130 Å (14). This is likely because we used the higher NaCl concentration and slightly alkaline pH that could reduce the overall size of CCL3 oligomers. However, CCL3 retained its rod-shaped, polydisperse oligomeric structure (Figure 2B). We also performed a SAXS analysis of CCL5(4-68) under the same

condition. However, the SAXS profile of CCL5(4-68) revealed significant aggregation, which precludes meaningful interpretation (Figure S2B).

Structure of heparin 8f-bound CCL5 and CCL3 oligomers: To address how GAG binds CCL5 oligomers, we solved a heparin **8f**-bound CCL5 hexamer structure. Anomalous signals confirmed the position of sulfate atoms in heparin **8f** (Figure S3A-B). For each CCL5(4-68) hexamer, two heparin **8f** chains that contained three sugar moieties were clearly visible (Figure 3A). The trisaccharide of **8f** binds a positively charged groove involving R17, K55, K56 and R59 of the CCL5(4-68) oligomer (Figure 3B). In addition to hydrogen bonds and van der Waals contacts, K55, K56 and R59 form a network of salt bridges with the sulfate groups of SGN-I, IDS-II, and SGN-III (Figure 3C, 3D). Thus, heparin primarily binds the ^{55}KKWVR^{59} motif of the CCL5 oligomer. This is consistent with the role of positively charged residue in the ^{55}KKWVR^{59} motif for GAG binding and biological functions, e.g. the adhesion of T lymphocytes and monocytes as well as leukocyte recruitment into the mouse peritoneal cavity (38). Previous analyses reveal that the ^{44}RKNR^{47} BBXB motif is known to be crucial for GAG binding and a structure to elucidate how heparin disaccharide binds this motif has been determined (18, 28, 34, 39). This BBXB motif, however, is largely buried in our CCL5 oligomer structure, which prevents it from binding heparin (Figure 3E, S3C). Thus, our structure indicates that the ^{55}KKWVR^{59} motif serves as the primary site to bind GAG when CCL5 is oligomerized. Our GAG-bound CCL5 structure suggested that the presence of heparin should significantly increase the propensity of CCL5 and CCL5(4-68) to form high MW aggregates. We probed the effect of heparin on CCL5 oligomerization by SAXS and found this to be the case (Figure S2).

We have also solved a heparin **8f**-bound CCL3 structure at 3.1Å resolution (Table S2, Figure S4). The structure contains five CCL3 monomers arranged similarly to the heparin-free CCL3 oligomer (14) and four sugar moieties in the **8f**-bound CCL3 structure (Figure 4A, S4). The CCL3 oligomers form a positively charged groove to bind heparin (Figure 4B). Taking advantage of the fact that the ^{45}KRSR^{48} BBXB motif is only partially buried, K45 and R46 from two different BBXB motifs of CCL3 monomers form salt bridges and van der Waals contacts with SGN-I in heparin **8f** (Figure 4C). In addition, Q19, N23, and K61 form salt bridges and hydrogen bonds with SGN-III and IDS-IV (Figure 4C, 4D). Furthermore, L66, D65 and Q22 form hydrophobic interactions with heparin **8f**. Interestingly, most residues involved in the binding of heparin to CCL3 and CCL5 oligomers are not well conserved despite the high conservation of residues involved in oligomerization (Figure 4E, 1E).

Alternative CCL3 oligomer structure: While seeking conditions to crystallize heparin-bound CCL3, we found a new crystallization condition that formed in the presence of **8f**. We optimized the condition without **8f** and solved an alternative CCL3 oligomer structure at 2.55Å resolution (Figure 5, Table S2, Figure S5A). This structure had 10 CCL3 molecules in an asymmetric unit, which forms a double helical rod-shaped oligomer that is similar to the previously reported CCL3 oligomer structure (14). However, four out of ten N-termini pass through the interface between CCL3 dimers and point outward towards the convex part of the CCL3 oligomer instead of pointing inward to the concave cavity of the CCL3 oligomer, as previously reported (Figure 5A) (14). While the outward pointing N-termini do not alter the overall structures of CCL3 monomers or dimers (except the N-termini) (Figure 5B), they push the CCL3 dimers apart, creating a larger gap (~3Å) between them (Figure 5C, S5B). As a result, salt bridges and hydrogen bonds between CCL3 dimers, including those between S33-Y15, E30-R18, D27-R46, and Y28-R48, are broken (Figure 5C). This leads to an overall loss of ~100Å^2 of contact surface between CCL3 dimers, thus likely reducing their affinity for each other (Figure 5C, S5C). However, the outward pointing N-termini of CCL3 form hydrogen bonds between A1-S33, S2-S33 and N34-L3, which help stabilize this structure. Interestingly, this N-terminal protrusion profoundly increases the size of the positively charged pocket on the CCL3 surface, which could bind GAG (Figure 5D). This might explain why **8f** facilitates the formation of this crystal form. However, no obvious extra density existed when CCL3 was co-crystallized with **8f**. This could be due to the low occupancy constrained by a crystal lattice and/or crystallization condition.

Discussion

Based on our crystallographic, SAXS, and mathematical modeling analyses, we propose that CCL5 oligomerization follows a simple polymerization process to form rod-shaped double helical oligomers that are polydisperse in size (Figure 6A). Despite being very different in their isoelectric points and charge distribution, CCL5 has the same mechanism of oligomerization with CCL3 and CCL4 (14). Our CCL5 oligomer structure explains existing CCL5 mutational data (15, 16, 18-21, 31). Furthermore, it offers an alternative model to describe how CXCL4 enhances the arrest of CCL5-stimulated monocytes (40, 41). Instead of hetero-dimerization between CCL5 and CXCL4 shown by NMR under an acidic condition (40), we propose that CXCL4 can form a hetero-oligomer with CCL5 (Figure S6). CXCL4 was discovered based on its high affinity to heparin, and our modeling predicts that this hetero-

oligomer would have altered electrostatic potential that could enhance GAG binding (Figure S6). In addition, the insertion of CXCL4 into CCL5 oligomer could also change the kinetics of CCL5 oligomerization. Together, they contributes to enhanced CCL5 function. This model is consistent with the available mutational data on the effects of ^{44}RKNR^{47} and E26 mutations (41). It suggests an exciting hypothesis that chemokine function is regulated by hetero-oligomerization of CC and CXC chemokines that typically form distinct dimers and higher-order oligomers (5).

Our GAG-bound CC chemokine structures reveal that a novel GAG binding site can form via protein oligomerization. Structures of CC chemokine oligomers reveal the molecular basis for how a positively charged pocket in the 50s loop of CCL5 binds GAGs even though the pocket formed by the BBXB motif in the 40s loop is buried. Furthermore, they show how a novel GAG binding site can form at the interface between CCL3 dimers. These structures offer a structural explanation for how multiple GAG binding sites can form upon CCL3 and CCL5 oligomerization and strengthen the binding of these chemokines to GAG via avidity. Consistent with this notion, the binding affinities of chemokines are highly dependent on oligomerization (42).

Our structural studies also offer additional mechanisms for regulating the coupling of oligomerization and GAG binding. We found an N-terminal flipped conformation of CCL3 within CCL3 oligomers, which likely occurs naturally due to the flexible nature of CCL3 N-terminus. This conformation has a reduced dimer-dimer interface, which should destabilize it relative to the non-flipped conformation and thus depolymerize more readily. This conformation, however, has a larger positively charged pocket so it could have a higher affinity for GAGs than the non-flipped conformation (Figure 5D). This is consistent with the fact that this crystal form is more readily formed when **8f** was present. Thus, the presence of GAG would promote the dissociation of CCL3 oligomers by weakening the interaction between CCL3 dimers. This offers a means by which conformational switches can regulate CCL3 oligomerization and explains how CCL3 forms shorter oligomers in the presence of heparin (14).

Our CCL5 oligomeric structure can, in part, explain how oligomerization affects CCL5 functions by affecting its proteolytic sensitivity (Figure 6A) (43). Only monomeric CC chemokines bind and activate their respective cognate CCRs. However, they are highly susceptible to proteolysis, particularly at their N-termini, which is critical for receptor binding

and activation (44-46). In comparison, CC chemokine oligomers are resistant to proteases but receptor-binding incompetent since oligomerization buries CCR-binding sites. Thus, dimerization and oligomerization prolong the half-life of CC chemokines while reducing the effectiveness of these chemokines. The N-terminus of CCL5 can be cleaved by DPP IV and cathepsin G, thus altering the ability of CCL5 to activate its cognate receptors (43). Our CCL5 oligomeric structure reveals that the CCL5 N-terminus is buried inside the concave surface of the oligomer, which should protect the oligomer from proteolytic inactivation. Oligomerization of CCL5 also buries substantial solvent-exposed areas. This should protect CCL5 from degradation by other extracellular proteases, e.g., tryptase (43). We have proposed that the interplay between reversible oligomerization and protease-sensitivity makes CCL3 and CCL4 more effective chemoattractants over a longer range and thus encodes severity during infection or inflammation (14) (Figure 6B). This is applicable to CCL5 and other chemokine that can oligomerize, e.g., CCL2.

GAG binding in conjunction with oligomerization can profoundly affect the functions of CC chemokines. Similar to oligomerization, GAG binding could alter the chemotactic gradient of CC chemokines by modulating their sensitivity to proteases (Figure 6C). GAG could bring multiple CC chemokine oligomers together (Figure 6C). Consistent with this notion, analysis of symmetry-related molecules in our structure indicates that long chain GAGs can bring two CCL3 oligomers together (Figure S4B-C). GAG-mediated aggregation of CC chemokine oligomers could further increase the local concentration of CC chemokines to regulate the activation of cognate CCRs and the presentation of CC chemokines to circulating lymphocytes (Figure 6C). This would also promote the formation of high MW CC chemokine oligomers in the extracellular matrix and on cell surfaces (Figure 6C). The oligomerization of CC chemokines and novel GAG binding of CC chemokine oligomers could facilitate the aggregation of proteoglycan, e.g., CD44, which in turn promotes non-CCR mediated signaling, e.g., tyrosine phosphorylation (Figure 6C). Given the complexity of how chemokines recruit immune cells, which involves cell arrest and adhesion onto the endothelial cells, extravasation across blood vessels, and cell migration toward the source of the CC chemokines, future investigation will be required to elucidate how the GAG binding and oligomerization of CC chemokines are coupled to affect each step of chemokine-mediated cell recruitment under normal physiological and pathological settings.

Methods

Chemokine expression and purification, crystallization, data collection, and structure determination: The expression of thioreduxin-tagged CCL5, CCL5(4-68), and CCL3 in *E. coli*, the removal of thioreduxin-tag by enterokinase or TEV protease, and the purification of these chemokines by Ni-NTA, source-Q, and heparin columns are done similar to methods described previously (14, 47). The octasaccharide heparin, MLZ-**8f** was synthesized as described (35). Crystals of CC chemokines in the presence and absence of heparin **8f** were grown using hanging drop vapor diffusion and cryo-protected under the conditions listed in Table S2. Diffraction data were collected at 100 K at beamline 19-ID or 19-BM at Advanced Photon Source, Argonne National Laboratory and processed with HKL3000 (48). Molecular replacement was done using PHASER (49) and structural refinement and rebuilding were performed with COOT (50) and PHENIX (51-53). Further details are provided in supplemental methods.

SAXS Data Acquisition and Analysis - SAXS data were collected at the BioCAT/18ID beamline at Advanced Photon Source, Argonne National Laboratory. Chemokine (0.6 mg/ml CCL5, 0.9 mg/ml CCL5(4-68), and 1 mg/ml CCL3) in the presence or absence of 1-10 μg/ml heparin (Alfa Aesar) in the buffer containing 20 mM Tris-HCl (pH 8.0), 500 mM NaCl, 1mM EDTA and 1mM β-mercaptoethanol was used for data collection. ATSAS package, Primus, and Crysol were used for data reduction and analysis (53, 54). A simple scheme for polymerization assuming equal probability of binding or unbinding between dimers independent of location was used to generate a model of oligomer size distribution to fit the SAXS data (14, 37). Further details are provided in supplemental methods.

Acknowledgements: We are grateful to Andrew Wang, John King, Mara Farcasanu, Stephanie Tang, and Krishna Rajarathnam for the helpful comments and the staff of APS SBC and BioCAT in assisting data collection. This work was supported by NIH grants GM81539, Institute of Translational Medicine (CTSA UL1 TR000430), and the University of Chicago BSD bridge funding to W.-J. Tang and Mizutani Foundation for Glycoscience, Academia Sinica, the Ministry of Science and Technology of Taiwan (104-0210-01-09-02 & 104-2628-M-001-001) to S.-C. Hung, P41 GM103622 to BioCAT, and training grants NIH (T32EB009412) and NSF (DGE-1144082). Use of the Advanced Photon Source was supported by the U.S. Department of Energy, Office of Basic Energy Sciences, under contract No. W-31-109-ENG-38.

References

1. Allen SJ, Crown SE, & Handel TM (2007) Chemokine: receptor structure, interactions, and antagonism. *Annu Rev Immunol* 25:787-820.
2. Lazennec G & Richmond A (2010) Chemokines and chemokine receptors: new insights into cancer-related inflammation. *Trends Mol Med* 16(3):133-144.
3. Xu D & Esko JD (2014) Demystifying heparan sulfate-protein interactions. *Annu Rev Biochem* 83(1):129-157.
4. Handel TM, Johnson Z, Crown SE, Lau EK, & Proudfoot AE (2005) Regulation of protein function by glycosaminoglycans--as exemplified by chemokines. *Annu Rev Biochem* 74:385-410.
5. Koenen RR & Weber C (2010) Therapeutic targeting of chemokine interactions in atherosclerosis. *Nature reviews. Drug discovery* 9(2):141-153.
6. Varki A*, et al.* (2009) *Essentials of Glycobiology* (Cold Spring Harbor (NY)) 2nd Ed.
7. Salanga CL & Handel TM (2011) Chemokine oligomerization and interactions with receptors and glycosaminoglycans: The role of structural dynamics in function. *Exp Cell Res* 317(5):590-601.
8. Fu L, Suflita M, & Linhardt RJ (2015) Bioengineered heparins and heparan sulfates. *Adv Drug Deliv Rev* ePub.
9. Jones KL, Maguire JJ, & Davenport AP (2011) Chemokine receptor CCR5: from AIDS to atherosclerosis. *Br J Pharmacol* 162(7):1453-1469.
10. Kanzler I, Liehn EA, Koenen RR, & Weber C (2012) Anti-inflammatory therapeutic approaches to reduce acute atherosclerotic complications. *Curr Pharm Biotechnol* 13(1):37-45.
11. Clemons MJ*, et al.* (1998) A randomized phase-II study of BB-10010 (macrophage inflammatory protein-1α) in patients with advanced breast cancer receiving 5-fluorouracil, adriamycin, and cyclophosphamide chemotherapy. *Blood* 92(5):1532-1540.
12. Kanegasaki S, Matsushima K, Shiraishi K, Nakagawa K, & Tsuchiya T (2014) Macrophage inflammatory protein derivative ECI301 enhances the alarmin-associated abscopal benefits of tumor radiotherapy. *Cancer Res* 74(18):5070-5078.
13. Graham GJ*, et al.* (1994) Aggregation of the chemokine MIP-1α is a dynamic and reversible phenomenon. Biochemical and biological analyses. *J Biol Chem* 269(7):4974-4978.
14. Ren M*, et al.* (2010) Polymerization of MIP-1 chemokine (CCL3 and CCL4) and clearance of MIP-1 by insulin-degrading enzyme. *EMBO J* 29(23):3952-3966.
15. Czaplewski LG*, et al.* (1999) Identification of amino acid residues critical for aggregation of human CC chemokines macrophage inflammatory protein (MIP)-1α, MIP-1β, and RANTES. Characterization of active disaggregated chemokine variants. *J Biol Chem* 274(23):16077-16084.
16. Appay V, Brown A, Cribbes S, Randle E, & Czaplewski LG (1999) Aggregation of RANTES is responsible for its inflammatory properties. Characterization of nonaggregating, noninflammatory RANTES mutants. *J Biol Chem* 274(39):27505-27512.
17. Baltus T, Weber KSC, Johnson Z, Proudfoot AEI, & Weber C (2003) Oligomerization of RANTES is required for CCR1-mediated arrest but not CCR5-mediated transmigration of leukocytes on inflamed endothelium. *Blood* 102(6):1985-1988.
18. Proudfoot AEI*, et al.* (2003) Glycosaminoglycan binding and oligomerization are essential for the in vivo activity of certain chemokines. *Proc Natl Acad Sci USA* 100(4):1885-1890.

19. Appay V*, et al.* (2000) RANTES activates antigen-specific cytotoxic T lymphocytes in a mitogen-like manner through cell surface aggregation. *Int Immunol* 12(8):1173-1182.
20. Murooka TT*, et al.* (2006) CCL5-CCR5-mediated Apoptosis in T Cells: requirement for glycosaminoglycan binding and CCL5 aggregation. *J Biol Chem* 281(35):25184-25194.
21. Roscic-Mrkic B*, et al.* (2003) RANTES (CCL5) uses the proteoglycan CD44 as an auxiliary receptor to mediate cellular activation signals and HIV-1 enhancement. *Blood* 102(4):1169-1177.
22. Iida N*, et al.* (2010) Antitumor effect after radiofrequency ablation of murine hepatoma is augmented by an active variant of CC Chemokine ligand 3/macrophage inflammatory protein-1α. *Cancer Res* 70(16):6556-6565.
23. Wagner L*, et al.* (1998) β-chemokines are released from HIV-1-specific cytolytic T-cell granules complexed to proteoglycans. *Nature* 391(6670):908-911.
24. Øynebråten I*, et al.* (2015) Oligomerized, filamentous surface presentation of RANTES/CCL5 on vascular endothelial cells. *Sci Rep* 5:9261.
25. Chung CW, Cooke RM, Proudfoot AE, & Wells TN (1995) The three-dimensional solution structure of RANTES. *Biochemistry* 34(29):9307-9314.
26. Hoover DM*, et al.* (2000) The crystal structure of Met-RANTES: Comparison with native RANTES and AOP-RANTES. *Protein Pep Lett* 7(2):73-82.
27. Jin H, Kagiampakis I, Li P, & LiWang PJ (2010) Structural and functional studies of the potent anti-HIV chemokine variant P2-RANTES. *Proteins* 78(2):295-308.
28. Shaw JP*, et al.* (2004) The X-ray structure of RANTES: heparin-derived disaccharides allows the rational design of chemokine inhibitors. *Structure* 12(11):2081-2093.
29. Wang X, Watson C, Sharp JS, Handel TM, & Prestegard JH (2011) Oligomeric structure of the chemokine CCL5/RANTES from NMR, MS, and SAXS data. *Structure* 19(8):1138-1148.
30. Wilken J*, et al.* (1999) Total chemical synthesis and high-resolution crystal structure of the potent anti-HIV protein AOP-RANTES. *Chem Biol* 6(1):43-51.
31. Brandner B, Rek A, Diedrichs-Mohring M, Wildner G, & Kungl AJ (2009) Engineering the glycosaminoglycan-binding affinity, kinetics and oligomerization behavior of RANTES: a tool for generating chemokine-based glycosaminoglycan antagonists. *Protein Eng Des Sel* 22(6):367-373.
32. Raman R, Sasisekharan V, & Sasisekharan R (2005) Structural insights into biological roles of protein-glycosaminoglycan interactions. *Chem Biol* 12(3):267-277.
33. Zulueta MML, Lin S-Y, Hu Y-P, & Hung S-C (2013) Synthetic heparin and heparan sulfate oligosaccharides and their protein interactions. *Curr Opin Chem Biol* 17(6):1023-1029.
34. Lortat-Jacob H, Grosdidier A, & Imberty A (2002) Structural diversity of heparan sulfate binding domains in chemokines. *Proc Natl Acad Sci USA* 99(3):1229-1234.
35. Zulueta MML*, et al.* (2012) α-Glycosylation by D-glucosamine-derived donors: synthesis of heparosan and heparin analogues that interact with mycobacterial heparin-binding hemagglutinin. *J Am Chem Soc* 134(21):8988-8995.
36. Hu Y-P*, et al.* (2012) Divergent synthesis of 48 heparan sulfate-based disaccharides and probing the specific sugar-fibroblast growth factor-1 interaction. *J Am Chem Soc* 134(51):20722-20727.
37. Vandongen PGJ & Ernst MH (1984) Kinetics of Reversible Polymerization. *J Stat Phys* 37(3-4):301-324.
38. Segerer S*, et al.* (2009) The basic residue cluster 55KKWVR59 in CCL5 is required for in vivo biologic function. *Mol Immunol* 46(13):2533-2538.

39. Proudfoot AE*, et al.* (2001) The BBXB motif of RANTES is the principal site for heparin binding and controls receptor selectivity. *J Biol Chem* 276(14):10620-10626.
40. Koenen RR*, et al.* (2009) Disrupting functional interactions between platelet chemokines inhibits atherosclerosis in hyperlipidemic mice. *Nat Med* 15(1):97-103.
41. von Hundelshausen P*, et al.* (2005) Heterophilic interactions of platelet factor 4 and RANTES promote monocyte arrest on endothelium. *Blood* 105(3):924-930.
42. Dyer DP, Salanga CL, Volkman BF, Kawamura T, & Handel TM (2015) The dependence of chemokine-glycosaminoglycan interactions on chemokine oligomerization. *Glycobiology* ePub.
43. Mortier A, Gouwy M, Van Damme J, & Proost P (2011) Effect of posttranslational processing on the in vitro and in vivo activity of chemokines. *Exp Cell Res* 317(5):642-654.
44. Paavola CD*, et al.* (1998) Monomeric monocyte chemoattractant protein-1 (MCP-1) binds and activates the MCP-1 receptor CCR2B. *J Biol Chem* 273(50):33157-33165.
45. Qin L*, et al.* (2015) Crystal structure of the chemokine receptor CXCR4 in complex with a viral chemokine. *Science* 347(6226):1117-1122.
46. Kufareva I, Salanga CL, & Handel TM (2015) Chemokine and chemokine receptor structure and interactions: implications for therapeutic strategies. *Immunol Cell Biol* 93(4):372-383.
47. Liang WG, Ren M, Zhao F, & Tang W-J (2015) Structures of human CCL18, CCL3, and CCL4 reveal molecular determinants for quaternary structures and sensitivity to insulin-degrading enzyme. *J Mol Biol* 427:1345-1358.
48. Minor W, Cymborowski M, Otwinowski Z, & Chruszcz M (2006) HKL-3000: the integration of data reduction and structure solution - from diffraction images to an initial model in minutes. *Acta Crystallogr D* 62:859-866.
49. McCoy AJ*, et al.* (2007) Phaser crystallographic software. *J Appl Crystallogr* 40(Pt 4):658-674.
50. Emsley P & Cowtan K (2004) Coot: model-building tools for molecular graphics. *Acta Crystallogr D Biol Crystallogr* 60(Pt 12 Pt 1):2126-2132.
51. Afonine PV*, et al.* (2012) Towards automated crystallographic structure refinement with phenix.refine. *Acta Crystallogr D Biol Crystallogr* 68(Pt 4):352-367.
52. Terwilliger TC*, et al.* (2009) Decision-making in structure solution using Bayesian estimates of map quality: the PHENIX AutoSol wizard. *Acta Crystallogr D Biol Crystallogr* 65(Pt 6):582-601.
53. Konarev PV, Volkov VV, Sokolova AV, Koch MH, & Svergun DI (2003) PRIMUS: a Windows PC-based system for small-angle scattering data analysis. *J Appl Crystallogr* 36(5):1277-1282.
54. Petoukhov MV*, et al.* (2012) New developments in the program package for small-angle scattering data analysis. *J Appl Crystallogr* 45(Pt 2):342-350.
55. Svergun D, Barberato C, & Koch M (1995) CRYSOL-a program to evaluate X-ray solution scattering of biological macromolecules from atomic coordinates. *J Appl Crystallogr* 28(6):768-773.

Figure Legends

Figure 1 Structure of CCL5(4-68) oligomer. A) Ribbon representation of CCL5(4-68) hexamer (PDB=5CMD). B) Detailed interactions between CCL5 dimers. C) Charge complementarity between CCL5 dimers and CCL3 dimers. The dimer interface is colored from negative surface (red, -1kT) to positive (blue +1kT). D) Comparison of CCL5 and CCL3 20mer. The PDB code of CCL3 oligomer is 2X69. Electrostatic surface is colored as calculated by APBS (< -1kT in red and > +1kT in blue). The 20mer models of CCL5 and CCL3 are built by the offset alignment and the use of symmetry related structure, respectively. E) Sequence alignment of CCL5 and CCL3. Identical and conserved residues are in red and boldface, respectively. Blue and cyan arrows indicate residues that form hydrophilic and hydrophobic interactions between CCL dimers, respectively.

Figure 2 SAXS scattering curve with cross-section, Guinier rod plot in inset (left) and the pair distribution (right) of CCL5 (A) and CCL3 (B). CCL5 data is fit with the fixed length oligomers of three CCL5 structure models, 5CMD-26mer (26mer of CCL5 structure with pdb code=5CMD), 2L9H-14mer, and 2VXW-28mer, which structures are shown as ribbon representation at the bottom of panel A. The length is chosen based on the optimal fitting χ values of 1.16, 1.91, and 2.03 for CCL5 5CMD-26mer, 2L9H-14mer, and 2VXW-28mer, respectively where χ was calculated by $\chi^2 = (1/(N-1)) \times \Sigma_j((\mu I(s_j) - I_{exp}(s_j))/\sigma(s_j))^2$ (N is the number of experimental points and μ is the scaling factor). Data is also fit with the mathematical model for the formation of double helical oligomers that are polydisperse in size (Polydisperse) using the equation for the concentration of oligomers of *k* monomers is $c(k) = \frac{c_t}{2}(1-\alpha^2)\alpha^{\left(\frac{k}{2}-1\right)}$, where α, the only fitting parameter, is directly related to the dissociation constant between dimers and c_t is the total protein concentration. The same process is used to analyze CCL3 SAXS data with either CCL3 10mer structure (pdb=2X69) (2X69-10mer) or a simple polymerization model that lead to the formation of CCL3 oligomers polydiperse in size (Polydiperse).

Figure 3 Structure of heparin **8f**-bound CCL5 hexamer. (A) Overall structure of **8f**-bound CCL5 oligomer. CCL5 is shown in ribbon representation and colored by chain. Carbon (yellow), oxygen (red), nitrogen (blue) and sulfur (orange) of heparin are depicted in stick. (B) Electrostatic potential is colored from red (-10kT) to blue (+10kT). (C) Close-up view and (D) schematic representation of the interaction of CCL5 and heparin **8f**. Red “eyelashes” indicate

hydrophobic interactions. (E) Ribbon representation of heparin disaccharide I-S bound CCL5 dimer (PDB=1U4L).

Figure 4 Structure of heparin **8f**-bound CCL3. A) Overall structure of **8f**-bound CCL3. CCL3 is shown in ribbon representation and colored by chain. Carbon (yellow), oxygen (red), nitrogen (blue) and sulfur (orange) of heparin are depicted in stick. B) Electrostatic potential is colored from red (-1kT) to blue (+1kT). (C) Close-up view and (D) schematic representation of the interaction of CCL3 and heparin **8f**. Red "eyelashes" indicate hydrophobic interactions. E) Sequence alignment of CCL5 and CCL3. Identical and conserved residues are in red and boldface, respectively. Cyan arrows indicate residues involved in the interaction of heparin with CCL3 while blue arrows indicate those with CCL5.

Figure 5 Structure of alternative CCL3 oligomer. (A) Ribbon representation of CCL3 decamer with four N-termini pointing outward and the comparison with CCL3 decamer with all N-termini pointing inward. (B) Alignment of monomer and dimer between CCL3 pointing outward and that pointing inward. Molecule is colored by RMSD. (C) Alignment of CCL3 with N termini pointing outward (colored, PDB=5COR) and that with N-termini inward (grey, PDB=2X69). Chain F was used for alignment. Chain F and Chain G have outward N-terminal. The close-up view shows gained hydrogen bonds (right, top) or lost hydrogen bonds (right, bottom) for CCL3 with N-termini pointing outward. D) Electrostatic surface potential of CCL3 decamer with N-termini pointing outward (top) and that with all N-termini pointing inward. The decamer surface is colored from negative (red -1kT) to positive (blue +1kT).

Figure 6 Roles of oligomerization, GAG binding, and proteolytic degradation of CC chemokines. (A) Equilibrium of CC chemokine oligomeric states and their properties in receptor binding and protease sensitivity. (B) Distribution of monomeric CC chemokine (log scale) from the source over the distance (linear scale). At low and medium levels of CC chemokine where it is most monomer or a mixture of monomer and dimer, respectively, cells will be directed to the center of CC chemokine source. However, at high CC chemokine level where it also forms oligomer, cells will only be migrated to the peripheral of CC chemokine source, rather than to the center. This would help to prevent the spread of invading pathogens in a severe infection. This is because the difference in CC chemokine monomer level within the cell length is less than required difference for the effective chemotaxis. (C) Effects of GAG binding and oligomerization to the functions of CC chemokines (see discussion).

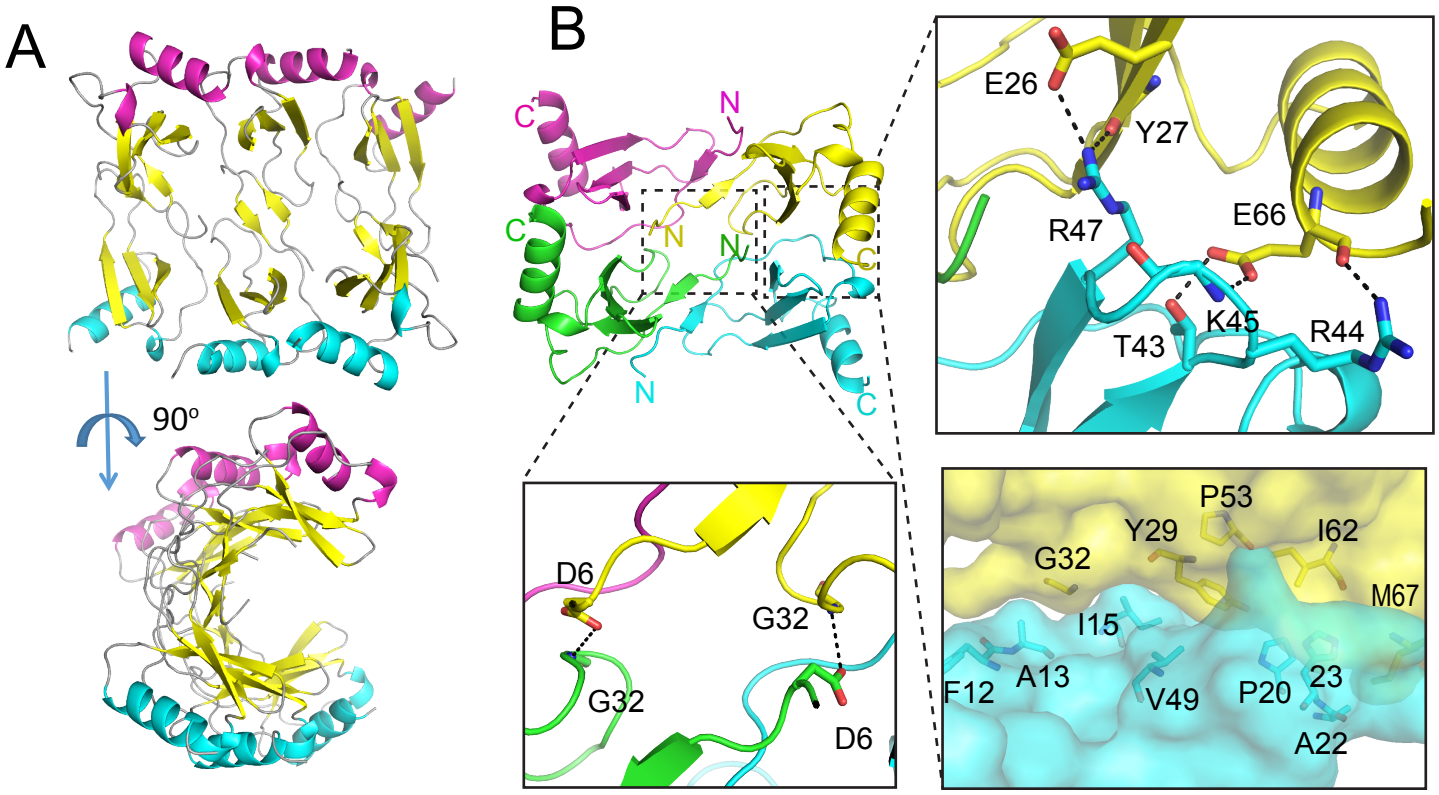

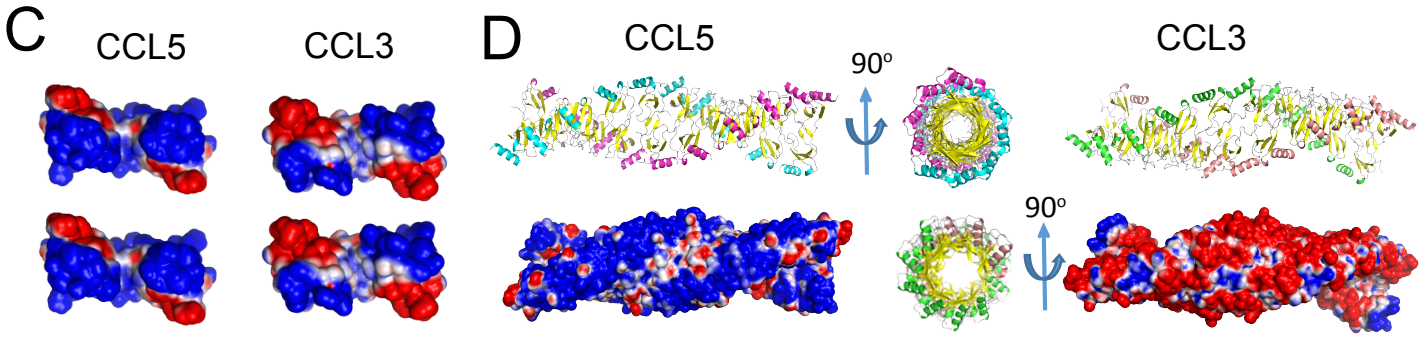

E

```
CCL5  SPYSSDTTPCCFAYIARPLPRAHIKEYFYTSGKCSNPAV
      1         10        20        30
CCL3  SLAADTPTACCFSYTSRQIPQNFIADYFETSSQCSKPGV

CCL5  VFVTRKNRQVCANPEKKWVREYINSLEMS
      40        50        60
CCL3  IFLTKRSRQVCADPSEEWVQKYVSDLELSA
```

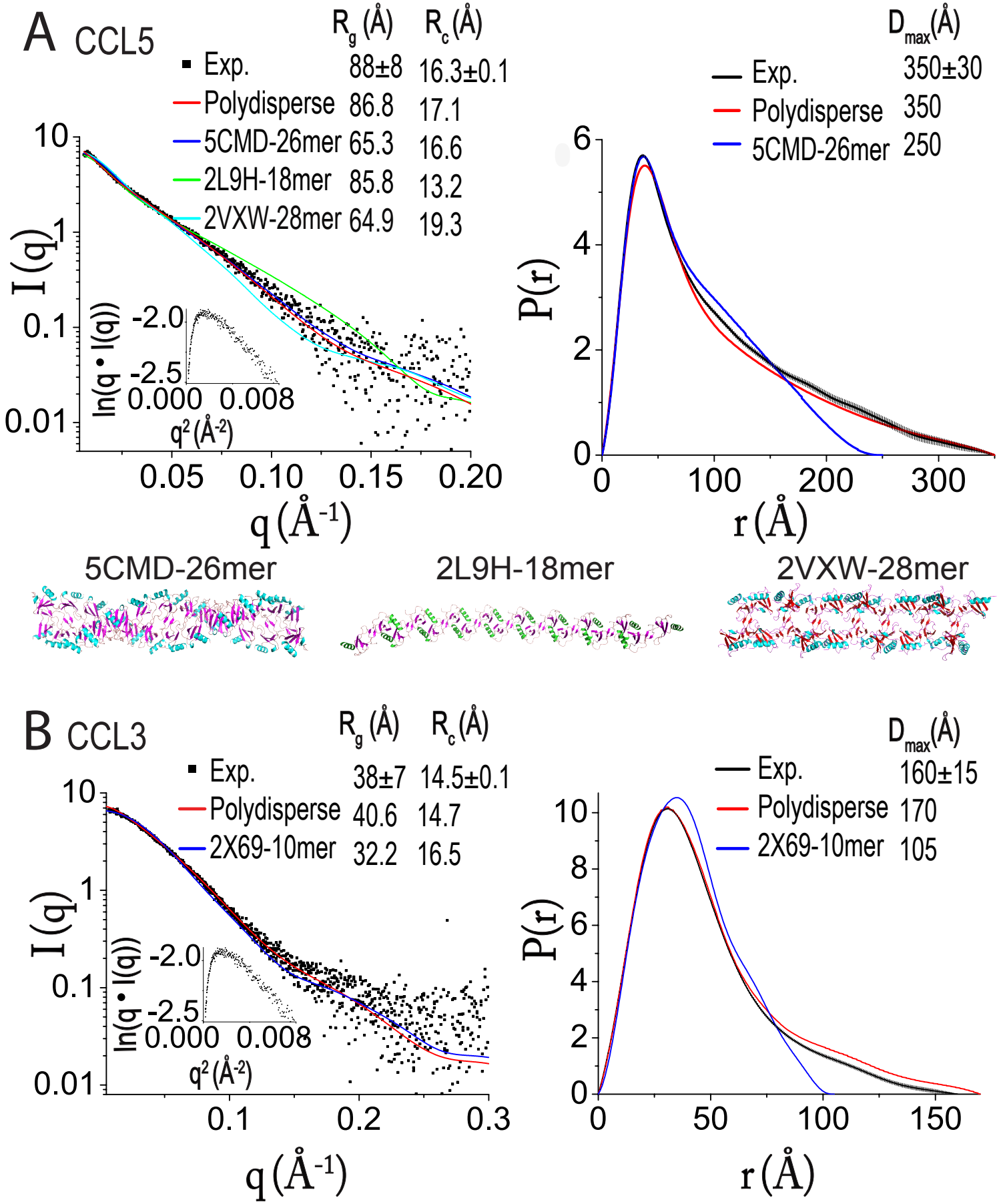
A CCL5
R_g (Å) R_c (Å)
Exp. 88±8 16.3±0.1
Polydisperse 86.8 17.1
5CMD-26mer 65.3 16.6
2L9H-18mer 85.8 13.2
2VXW-28mer 64.9 19.3
I(q)
q (Å^-1)
ln(q • I(q))
q² (Å⁻²)
D_max (Å)
Exp. 350±30
Polydisperse 350
5CMD-26mer 250
P(r)
r (Å)
5CMD-26mer
2L9H-18mer
2VXW-28mer
B CCL3
R_g (Å) R_c (Å)
Exp. 38±7 14.5±0.1
Polydisperse 40.6 14.7
2X69-10mer 32.2 16.5
I(q)
q (Å^-1)
ln(q • I(q))
q² (Å⁻²)
D_max (Å)
Exp. 160±15
Polydisperse 170
2X69-10mer 105
P(r)
r (Å)

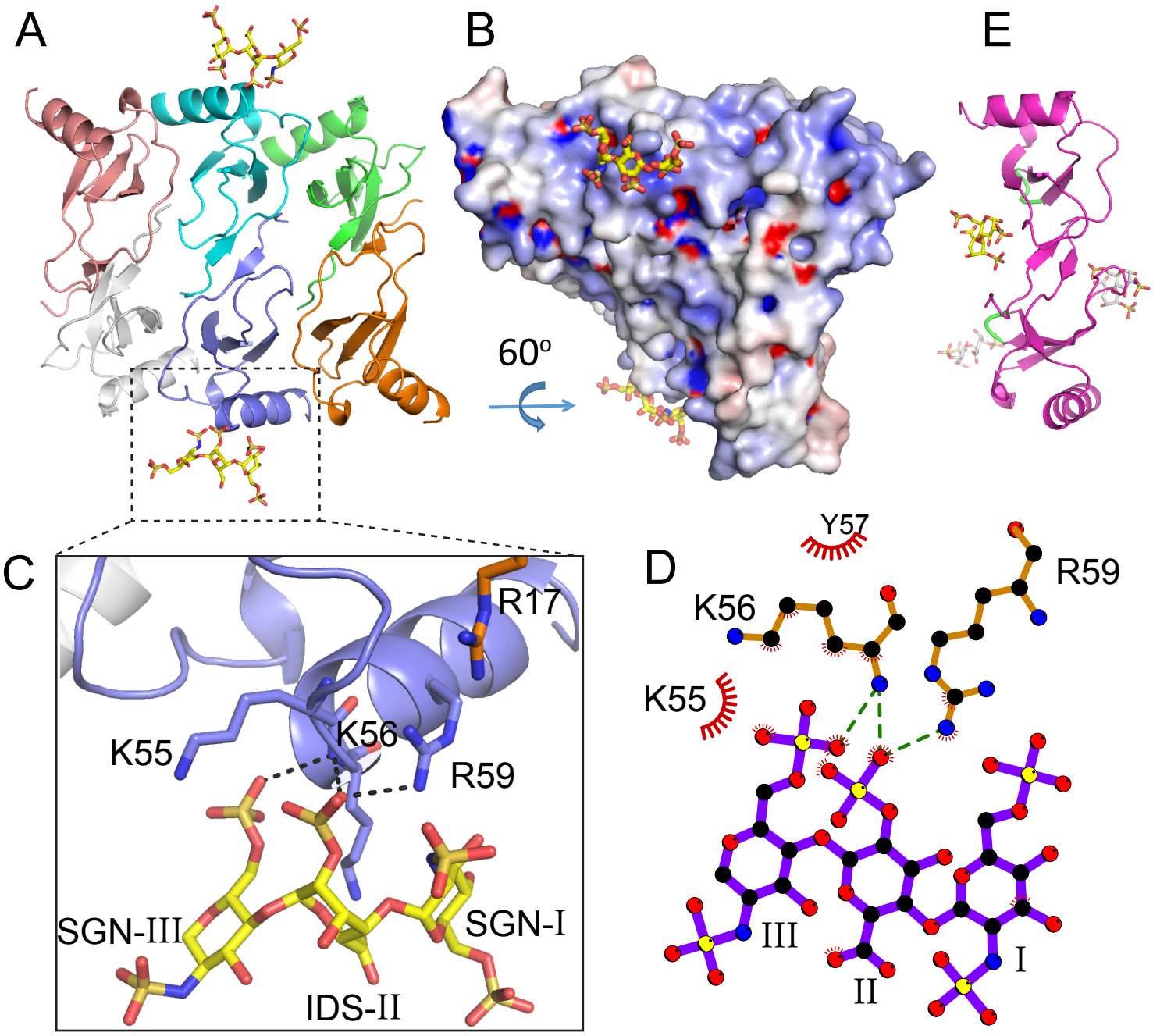
A
B
E
60º
C
R17
K55
K56
R59
SGN-III
SGN-I
IDS-II
D
Y57
K56
R59
K55
III
II
I

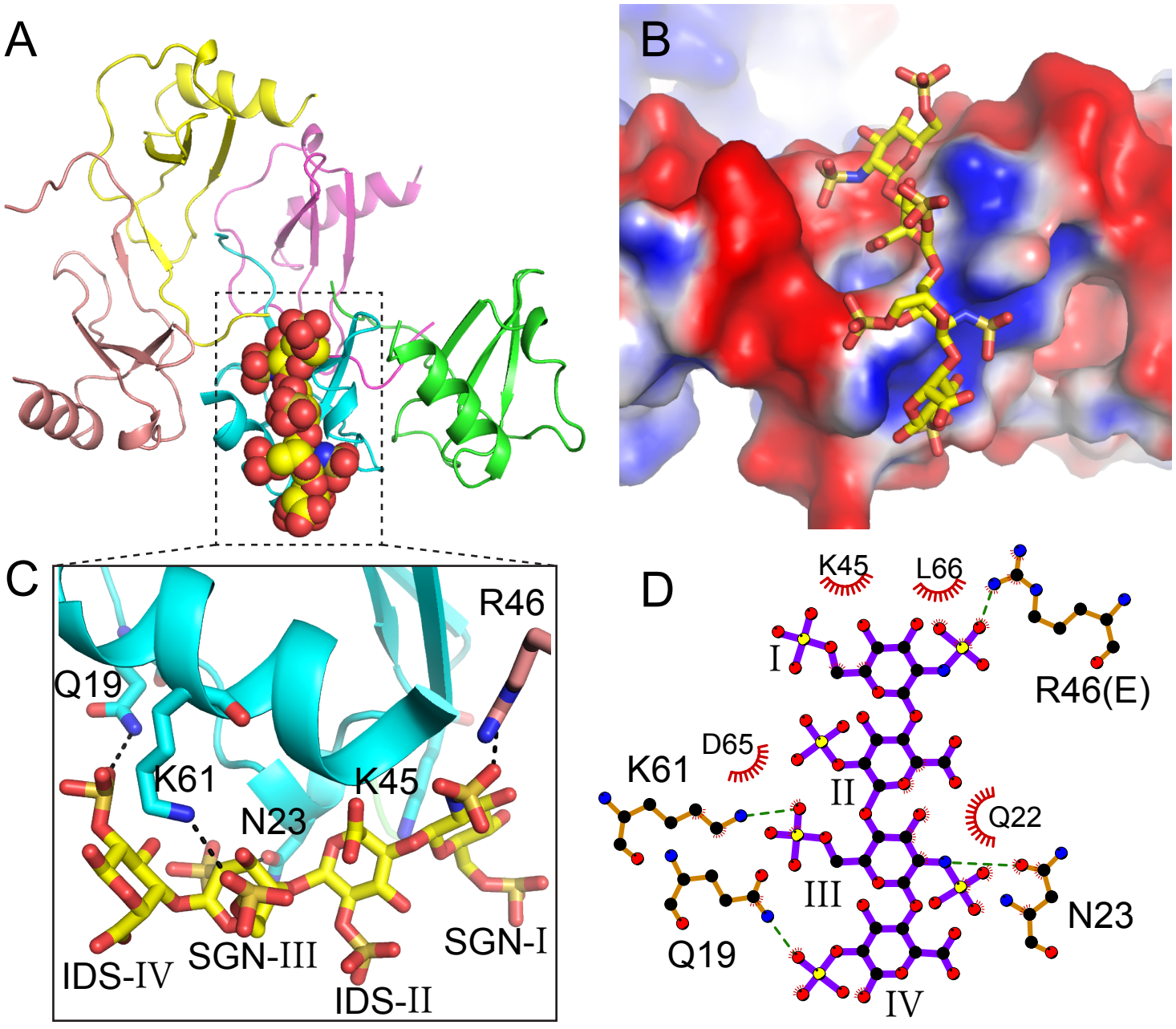

E

```
CCL5  SPYSSDTTPCCFAYIARPLPRAHIKEYFYTSGKCSNPAV
          1        10        20        30
CCL3  SLAADTPTACCFSYTSRQIPQNFIADYFETSSQCSKPGV

CCL5  VFVTRKNRQVCANPEKKWVREYINSLEMS
         40        50        60
CCL3  IFLTKRSRQVCADPSEEWVQKYVSDLELSA
```

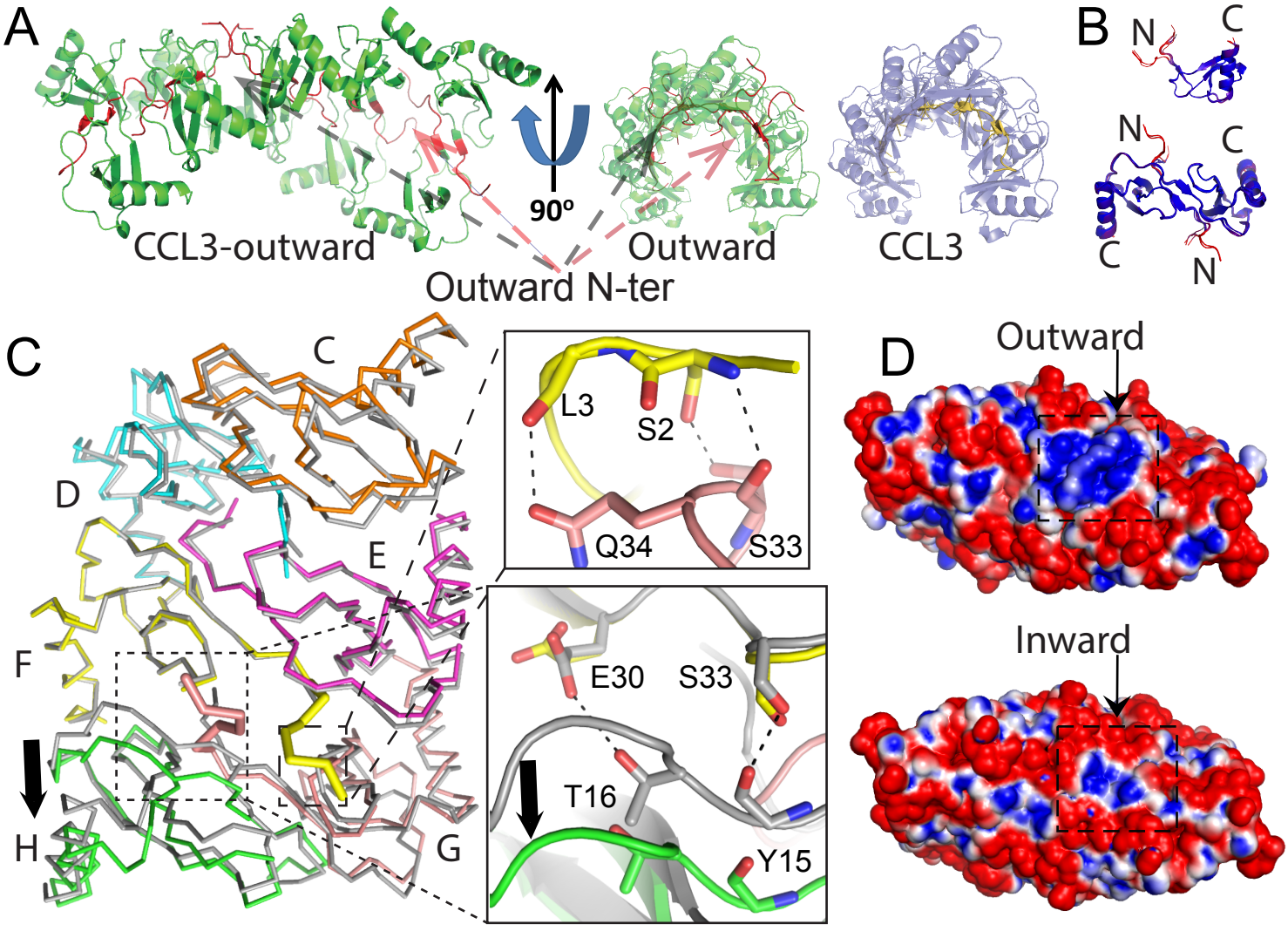
A
CCL3-outward
90º
Outward
Outward N-ter
CCL3
B
N
C
N
C
C
N
C
D
E
F
G
H
L3
S2
Q34
S33
E30
S33
T16
Y15
D
Outward
Inward

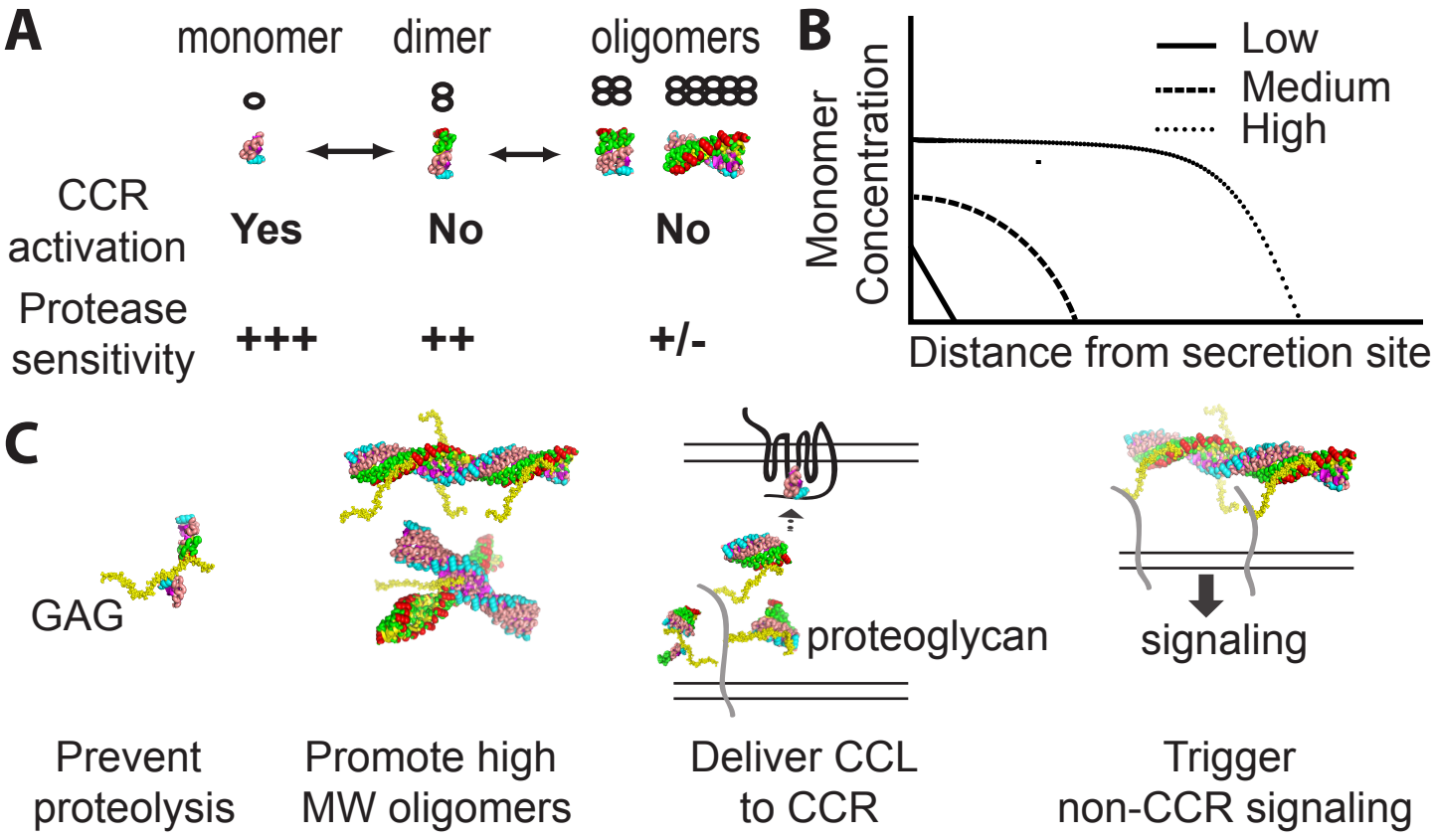
A
monomer
dimer
oligomers
CCR activation
Yes
No
No
Protease sensitivity
+++
++
+/-
B
Monomer Concentration
Low
Medium
High
Distance from secretion site
C
GAG
proteoglycan
signaling
Prevent proteolysis
Promote high MW oligomers
Deliver CCL to CCR
Trigger non-CCR signaling